15

Miscellaneous detectors and applications

15.1 Optical imaging chambers

The process of electron–molecule collisional photon emission, described in Chapter 5, is exploited in the gas scintillation proportional counters; with photo-multiplier readout, the devices detect the primary or the field-enhanced secondary gas scintillation, providing energy resolutions approaching the statistical limit for soft X-rays. At high charge gains, the photon emission is copious enough to permit the use of pixelated photon sensors, image intensifiers, solid state cameras and similar, for imaging the position of the radiation through a window and with suitable optics. While limited in rate by the recording hardware, optical imaging has the potential advantage of a high granularity at low cost.

In a TPC-like configuration, ionization released in the gas volume drifts to a charge-multiplying element; a suitable optics focuses the image on the sensor (Figure 15.1). Due to the long integration time of standard cameras, the recorded image corresponds to the projection of the tracks on the plane of the multiplier, integrated over the full drift time; addition of a photomultiplier to record the time structure of the light emission can provide further information on the event.

As the scintillation of most gases is peaked in the far or vacuum ultra-violet, in order to permit the use of cheap windows and sensors, the wavelength of the photon emission has to be shifted close to the visible range. This can be obtained with a thin layer of wavelength shifter (WLS) deposited on the inner side of the window, or more conveniently using an additive to the main gas acting as internal wavelength shifter. Early work in this direction, using acetone as internal WLS and an image intensifier as sensor, demonstrated the feasibility of the technique (Gilmore *et al.*, 1983).

The low-ionization threshold vapours studied in the development of the Cherenkov ring imaging technique, TEA and TMAE (see Chapter 14) are particularly efficient internal shifters, with a peak of emission under avalanche conditions
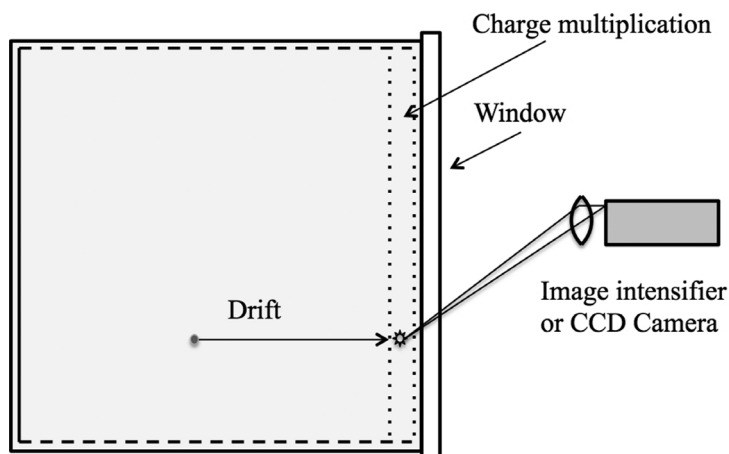
430

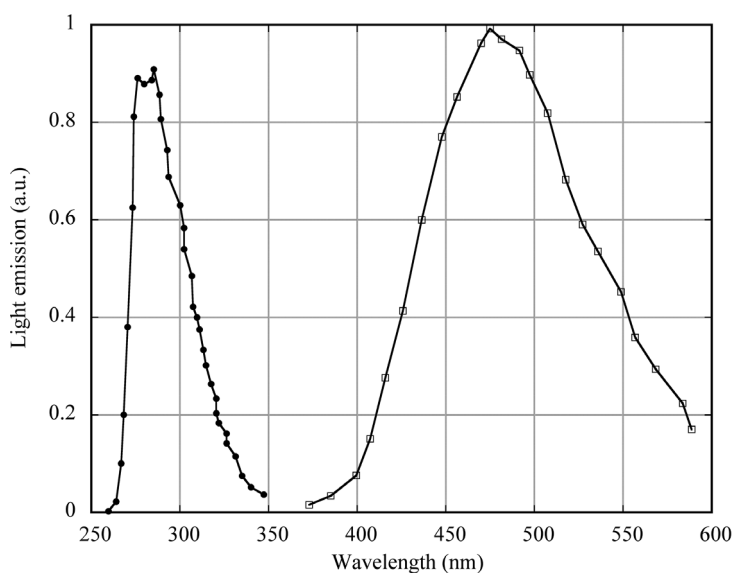Figure 15.1   Scheme of the optical imaging chamber.

Figure 15.2   Scintillation emission spectra of TEA and TMAE. Data from Suzuki *et al.* (1987) and Charpak *et al.*, (1988). By kind permission of Elsevier.

around 280 and 480 nm, respectively (Figure 15.2) (Suzuki *et al.*, 1987; Charpak *et al.*, 1988). Although the longer wavelength of the TMAE emission is easier to detect and image, the difficult manipulation and chemical reactivity have generally discouraged its use.

A standard MWPC with a gas filling containing 7% triethyl amine (TEA) was used in the early development of the optical imaging chamber; however, a parallel-plate single or multi-step structure appeared to be a better solution because of the
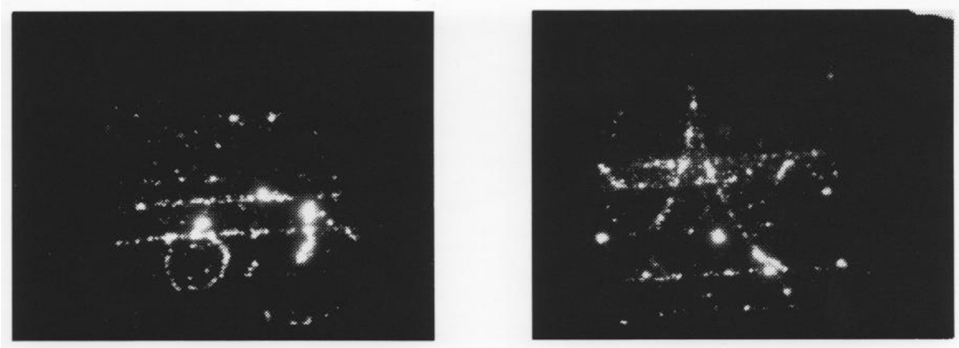
Figure 15.3　Cosmic ray activity recorded with the optical imaging chamber (Charpak *et al.*, 1987). By kind permission of Elsevier.
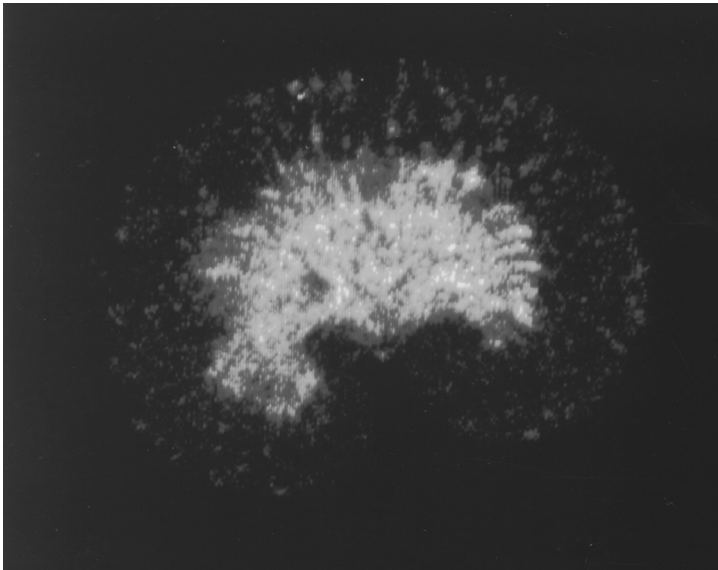

Figure 15.4　Autoradiography of a tritiated rat kidney slice recorded with the optical imaging chamber (Dominik *et al.*, 1989). By kind permission of Elsevier.

larger gains achievable and the uniform response, not modulated by the wire spacing; the photon emission close to the surface of the window reduces parallax errors, particularly when using a thin foil WLS (Charpak *et al.*, 1987; Suzuki *et al.*, 1988). Screen shots of cosmic ray activity recorded with a small optical imaging chamber are shown in Figure 15.3 (Charpak *et al.*, 1987).

The optical imaging chamber has been used for applications in several fields. The image in Figure 15.4 is the optical recording of the activity from a tritium-loaded slice of a rat's kidney, placed inside the detector over the cathode of a parallel plate
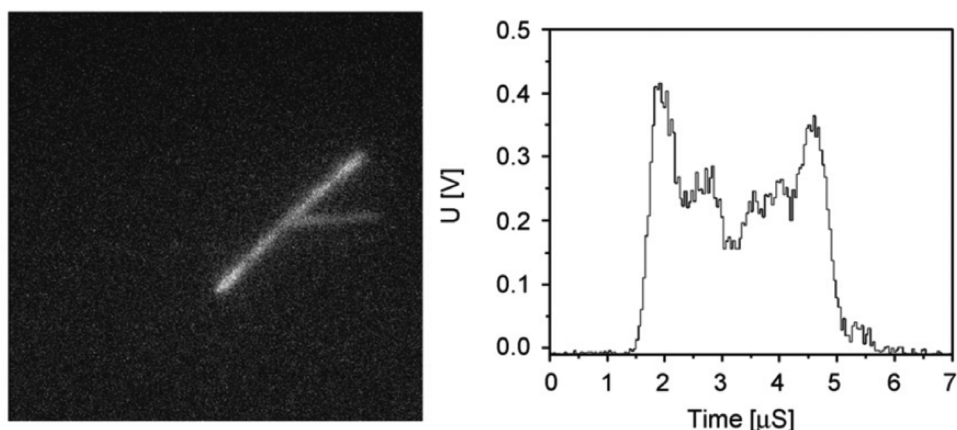
Figure 15.5   Projected image of a nuclear decay (left) and corresponding time distribution of the scintillation (right) (Miernik *et al.*, 2007). By kind permission of Elsevier.

avalanche counter; the exponential avalanche growth in the gap favours the localization of the emission point of the positron (Dominik *et al.*, 1989).

Other applications include the imaging of charged particle tracks for dosimetry (Titt *et al.*, 1998) and nuclear isotope decays (Cwiok *et al.*, 2005). As seen in Figure 15.5, a simultaneous recording of the projected tracks and of the time structure of the scintillation, detected with a photomultiplier operated synchronously with the imaging camera, provides information on the ionization density of the tracks (Miernik *et al.*, 2007).

The introduction in the late nineties of the gas electron multiplier (GEM), described in Section 13.4, opened up new possibilities for the development of optical imagers. Capable of achieving high proportional gains in ^{3}He-CF_4 gas mixtures, the devices have been used to image the proton–triton pairs issued by neutron conversions in the gas. While the main reason for adding carbon tetrafluoride to the detectors is to decrease the range of the ionizing prongs, it has been found that CF_4 has a strong scintillation component in the visible, between 500 and 700 nm, matching the spectral sensitivity of solid state CCD cameras, Figure 15.6 (Fraga *et al.*, 2002). Figure 15.7 is an image of multiple neutron interactions in the gas, showing several proton–triton pairs (Fraga *et al.*, 2002). Integration of the scintillation yield along the tracks permits the identification of the prongs; in the detection of ions stopping in the gas volume, the time dependence of the yield clearly shows the typical Bragg peak energy loss profile, Figure 15.8 (Margato *et al.*, 2004).

The very good proportionality between the scintillation yield and the energy loss of charged particles is also a promising tool for dose assessment in hadron therapy (Seravalli *et al.*, 2009; Klyancho *et al.*, 2012).
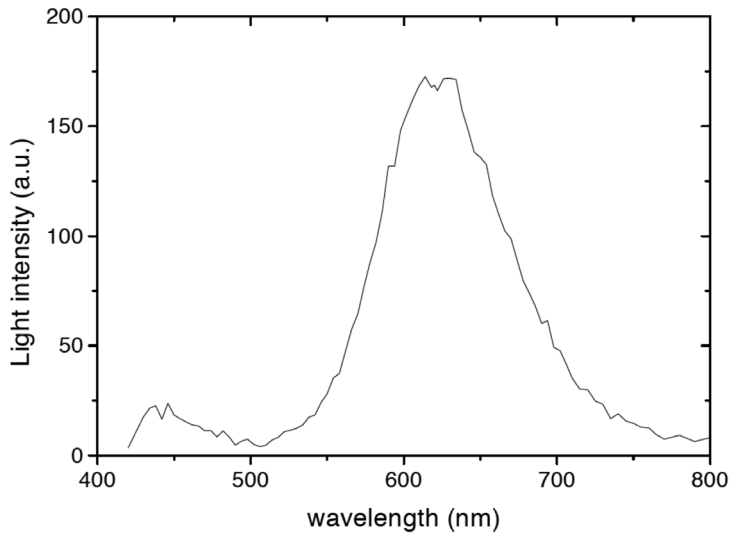
Figure 15.6 Scintillation yield of ^{3}He-CF$_4$, measured at a GEM charge gain of 190 (Fraga *et al.*, 2002). By kind permission of Elsevier.

Figure 15.7 Neutron interactions in ^{3}He detected with a GEM-based optical imaging chamber (Fraga *et al.*, 2002). By kind permission of Elsevier.

15.2 Cryogenic and dual-phase detectors

Liquid xenon is used as sensitive volume in a TPC-like configuration for applications requiring the detection of low interaction cross section events, exploiting its higher density and atomic number. Figure 15.9 shows the LXe Gamma-Ray
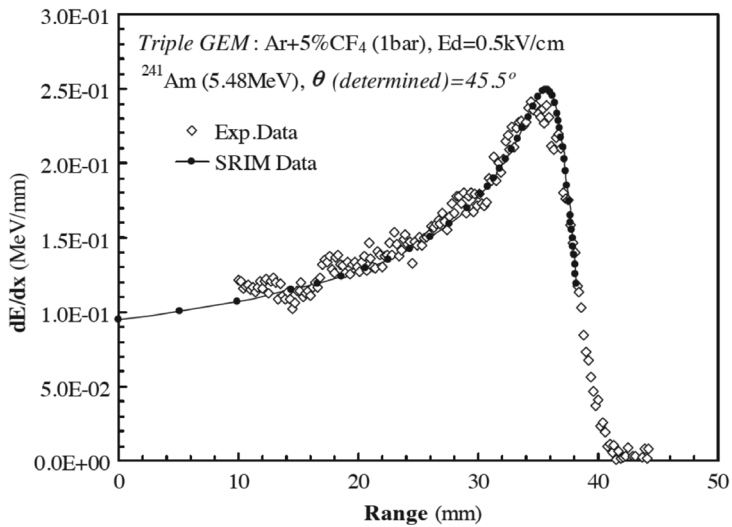
Figure 15.8   Computed (full line) and measured light yield for stopping 5.58 MeV alpha particles (Margato *et al.*, 2004). By kind permission of Elsevier.
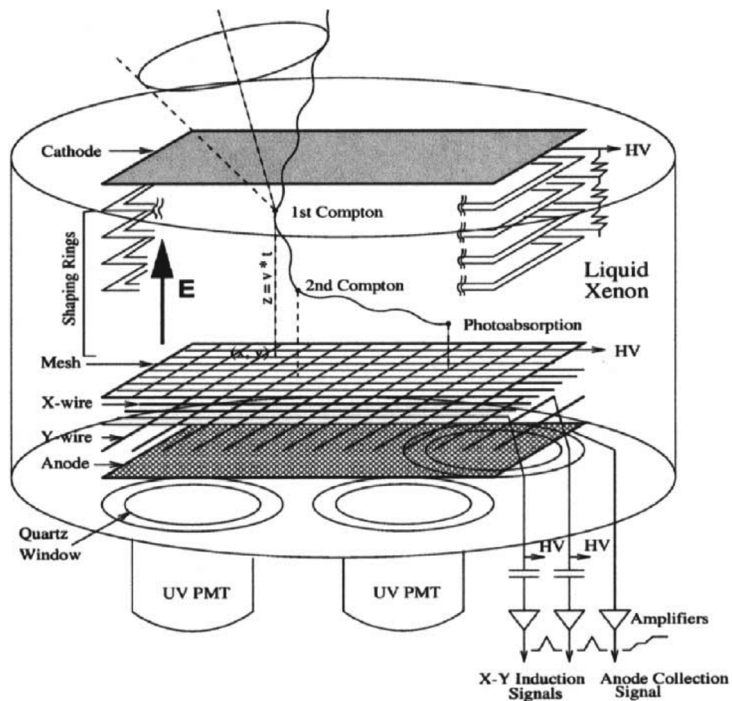

Figure 15.9   Scheme of the LXe GRIT TPC (Aprile *et al.*, 2001). By kind permission of Elsevier.
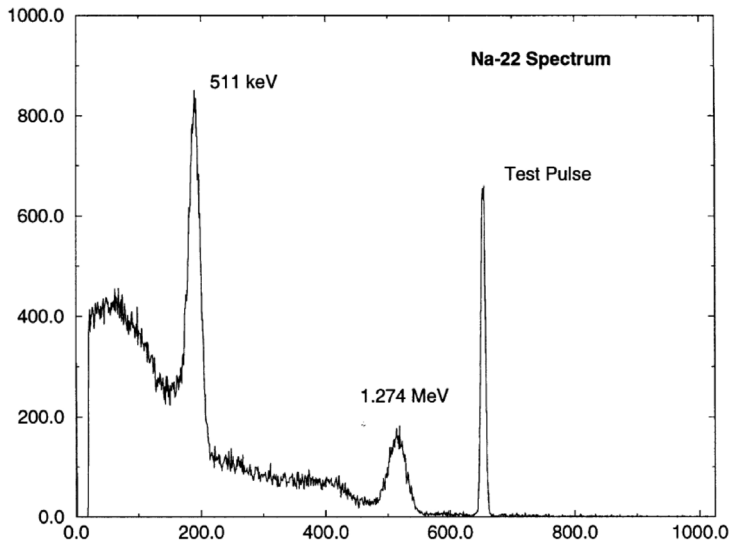
Figure 15.10   Energy resolution of the LXe TPC measured for a ^{22}Na source (Aprile *et al.*, 2002). By kind permission of Elsevier.

Imaging Telescope (GRIT), a cryogenic TPC developed for the imaging of high-energy gamma rays in balloon-borne astrophysics experiments (Aprile *et al.*, 2001). The detector, with 400 cm^3 sensitive area and 7 cm drift gap, is filled with high purity liquid xenon. UV-sensitive photomultipliers detect the primary scintillation and generate the event trigger, while the charge signals collected on two orthogonal wire meshes provide the three-dimensional image of the ionization trails. Systematic measurements demonstrate the energy and spatial resolution of the detector; Figure 15.10 is an example of the scintillation spectrum recorded with a ^{22}Na source (Aprile *et al.*, 2002). The device has been successfully tested for applications as Compton imager of gamma ray sources in astrophysics (Aprile *et al.*, 2008) exploiting the method outlined in Section 3.7. In later developments, the direct charge collection in the liquid has been replaced by the detection, on a second set of photomultipliers, of the secondary scintillation of electrons extracted from the liquid into an overlying gas layer and subject to a high electric field; other dual-phase devices are described below. A prototype detector, XENON10 (Sorensen *et al.*, 2009), and the larger sibling XENON100, with 65 kg of active LXe, operated in the Italian Gran Sasso Laboratory aiming at the detection of dark matter and weakly interacting massive particles (WIMPs); Figure 15.11 is an artist's view of XENON1T, an advanced project with a sensitive volume close to 1 ton (XENON). Similar in conception, the LUX dark matter detector, installed in a
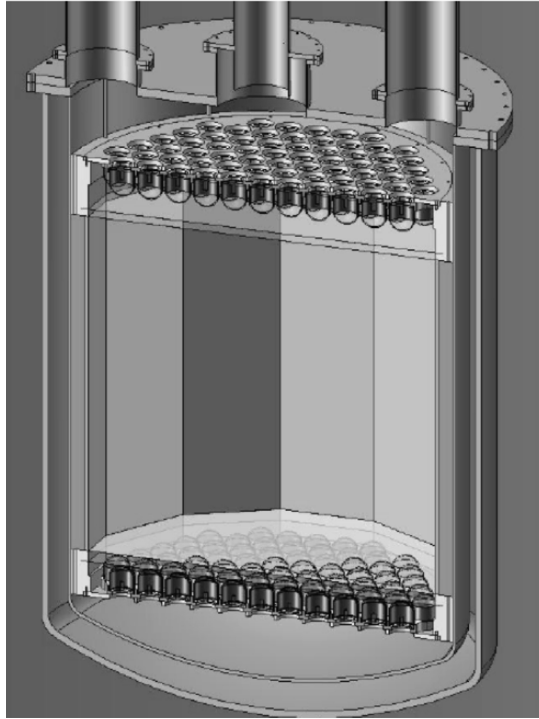
Figure 15.11 Artist's view of XENON1T, showing the cryostat with the LXe sensitive volume and the photomultiplier arrays to detect the primary scintillation in the liquid and the secondary emission from the gas (XENON). E. Aprile personal communication.

mine in South Dakota, has an active volume of 350 kg liquid xenon (LUX). Due to the very low expected event rate, if any, extreme care is devoted to the choice of the components and screenings to reduce the accidental counts due to radioactivity.

Alternatively to the use of external devices for detection of the scintillation, several successful attempts have been described which make use of internal CsI sensitive layers with extraction of the photoelectron in the liquid and successive transport and detection of the charge (Aprile *et al.*, 1994; Periale *et al.*, 2004).

Exploited in the devices described above, the dual-phase concept, where electrons are extracted from the liquid and amplified by charge multiplication in the gas phase, has been studied by many authors, in particular for applications in astrophysics and rare event detection (Bolozdynya, 1999; Aprile *et al.*, 2004).

The gains achievable in gases at cryogenic temperatures have been studied systematically by using as charge amplifying detectors gas electron multipliers
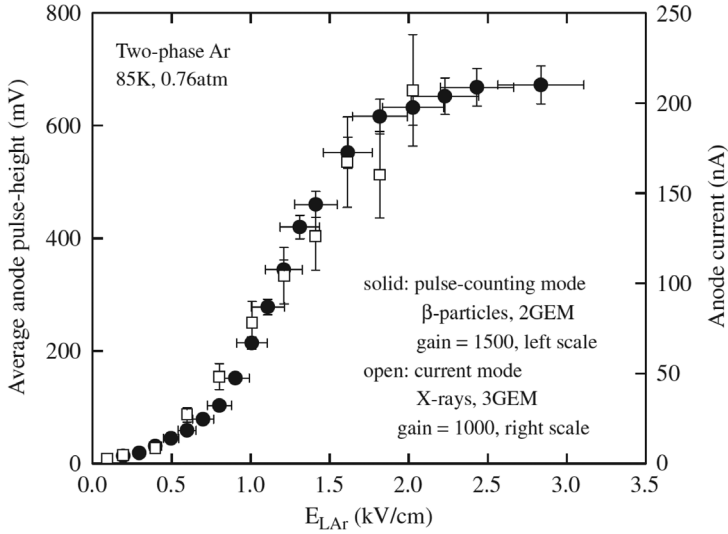
Figure 15.12   Electron extraction probability from liquid argon as a function of field, recorded in the pulse or current detection modes (Bondar *et al.*, 2006). By kind permission of Elsevier.
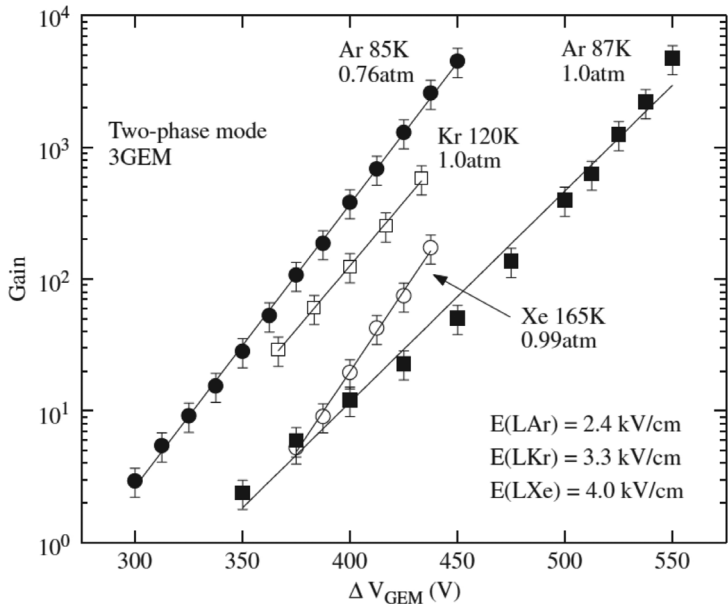

Figure 15.13   Two-phase gains measured with a triple-GEM as a function of voltage applied to each multiplier (Bondar *et al.*, 2006). By kind permission of Elsevier.
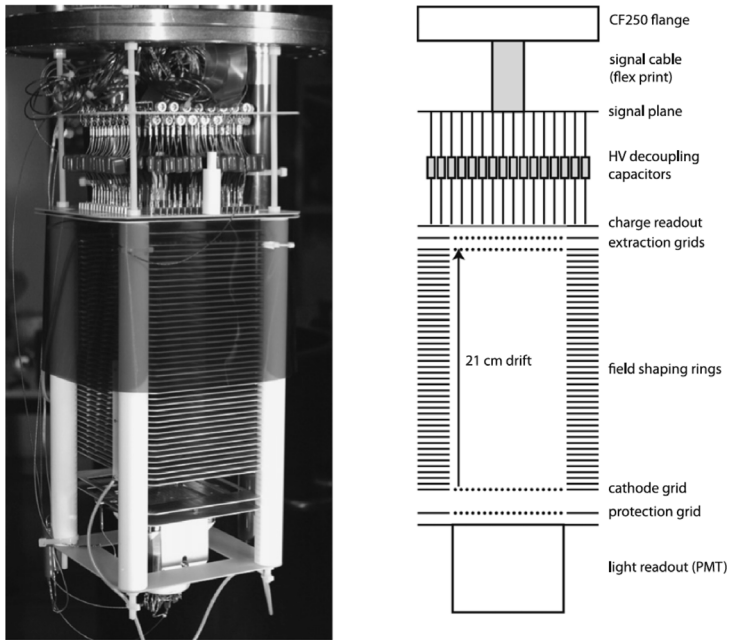
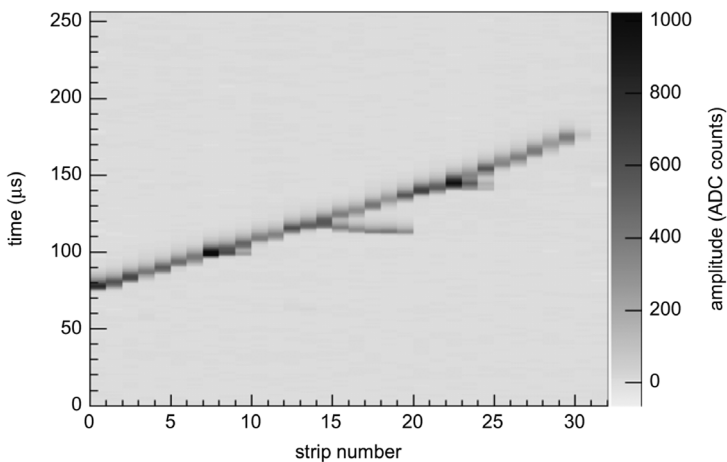Figure 15.14   The LAr LEM-TPC prototype (Badertscher *et al.*, 2011). By kind permission of Elsevier.

Figure 15.15   Muon track recorded with the LEM-TPC (Badertscher *et al.*, 2011). By kind permission of Elsevier.

(GEMs) in cascade (see Section 13.4), assembled at a short distance above the liquid level; the voltage applied to the lower GEM electrode facing the liquid controls the electron extraction probability. As shown in Figure 15.12, a full extraction from liquid argon is obtained at fields above 2 kV/cm (Bondar *et al.*,

2006). Figure 15.13, from the same reference, is an example of gains measured with a triple-GEM detector in argon, krypton and xenon at different temperatures and pressures in the two-phase operation, as a function of GEM voltage.

Several dual-phase detectors have been built making use of micro-pattern gaseous amplifying structures, aiming at neutrino and dark matter direct searches: Micromegas (Lightfoot *et al.*, 2005) and the coarser GEM structure named the large electron multiplier (Badertscher *et al.*, 2010). The liquid argon large electron multiplier time projection chamber (LAr LEM-TPC), shown in Figure 15.14, has a 21-cm long drift volume. A photomultiplier at the bottom end detects the primary scintillation, thus providing the energy trigger; ionized trails are drifted into the multiplier and detected on sets of perpendicular strips on the LEM readout plane. Figure 15.15 is an example of a muon track with delta rays recorded with the detector (Badertscher *et al.*, 2011).

A comprehensive summary of liquid noble gas detectors is given in Chepel and Araujo (2013).